Journal of Colloid and Interface Science 629 (2023) 694–704

Contents lists available at ScienceDirect

Journal of Colloid and Interface Science

journal homepage: www.elsevier.com/locate/jcis

Regular Article

Tailoring the humidity response of cellulose nanocrystal-based films by specific ion effects

Maoqi Lin [a], Vikram Singh Raghuwanshi [a], Christine Browne [a], George P. Simon [b], Gil Garnier [a,*]

[a] Bioresource Processing Research Institute of Australia (BioPRIA), Department of Chemical and Biological Engineering, Monash University, Clayton, VIC 3800, Australia
[b] Department of Materials Science and Engineering, Monash University, Clayton, VIC 3800, Australia

GRAPHICAL ABSTRACT

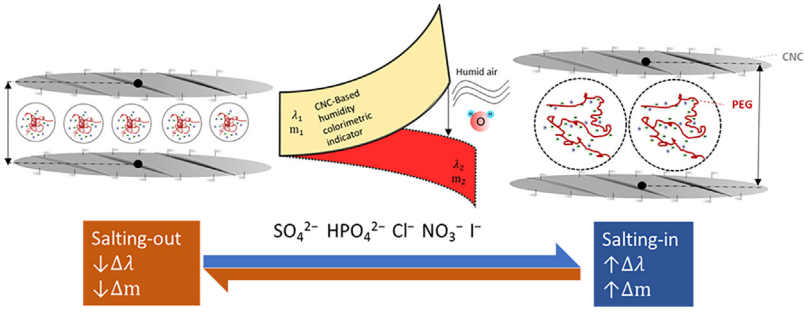

ARTICLE INFO

Article history:
Received 18 August 2022
Revised 15 September 2022
Accepted 19 September 2022
Available online 24 September 2022

Keywords:
Specific ion effect
Humidity response
Cellulose nanocrystal composites
polyethylene glycol (PEG)

ABSTRACT

Hypothesis: The optical properties and humidity response of iridescent films made of cellulose nanocrystal (CNC) and polyethylene glycol (PEG) can be tailored by the incorporation of electrolytes chosen based on specific ion effects (SIE).

Experiments: A series of inorganic salts comprising five different cations and five anions based on the Hofmeister series were mixed with CNC/PEG suspensions, followed by an air-dried process into iridescent solid films. These films were tested in changing relative humidity (RH) environments from 30% to 90% and their photonic properties and mass change monitored. The underlying structures and the mechanism of their formation were quantified in terms of interparticle distance derived from small angle X-ray scattering experiment and pitch size quantified by scanning electron microscope (SEM).

Findings: The specific color and color range of CNC/PEG based films are controlled by a specific anion effect achieved by selection of the salt while the specific cation effect is negligible. The salting-in type anions with the same valency result in a red-shift color when films are in the dried state. The salting-in type leads to a greater color changing range during RH changes than the salting-out type. The resultant mass gain/loss trend is consistent with the color change. In contrast, cations do not show any relationships between salting-in effect and the measured properties as observed for anions. The observed SIE can be used to engineer CNC/polymer-based humidity and bio-diagnostic colorimetric indicator devices.

1. Introduction

Cellulose nanocrystals (CNC) are extracted and refined from lignocelluloses plants, tunicate and bacteria. Their inherent renewability and biodegradability have attracted much interest and

* Corresponding author.
E-mail address: Gil.Garnier@monash.edu (G. Garnier).

https://doi.org/10.1016/j.jcis.2022.09.101
0021-9797/

Abbreviations and Nomenclatures

CCC	critical coagulation concentrations
CNC	Cellulose NanoCrystal
CN*	Chiral Nematic
Da	Dalton
KW	kilowatts
PEG	PolyEthylene Glycol
MW	Molecular Weight
MΩ·cm	million-ohm times centimeter
RH	Relative Humidity
SAXS	Small Angle X-ray Scattering
SD	Standard deviation
SEM	Scanning Electron Microscope
SIE	Specific Ion Effects
UV-NIR	Ultraviolet-Near Infrared
$\boldsymbol{d}$	Interparticle distance
$\boldsymbol{P}$	Pitch
$\boldsymbol{\lambda_{max}}$	Maximum wavelength (peak)
$\boldsymbol{\Delta m}$	Mass changes
$\frac{\partial \boldsymbol{m}(\%)}{\partial \boldsymbol{t}}$	Mass responsive rate

device development in recent years [1–3]. Among such CNC applications are photonic crystals which demonstrate structural color [3]. Aqueous suspensions of acid-hydrolyzed CNC form a periodic arrangement as their concentration increases due to their high surface charge and is retained as the film is dried. During the film formation upon the suspension drying, the CNC particles pass from an isotropic phase with random orientation, into a liquid crystalline structures in the nematic state with parallel alignment, and subsequently into a chiral nematic phase (denoted as CN*) where the CNC rods form helical structures at a mesoscopic level in the final liquid state prior to final solidification. When the tactoids are fully dried, the CN* structure is retained and becomes iridescent when illuminated by ambient light. This is because each CNC possesses a slightly rotated position relative to its neighbor through the depth direction of the film. The length over a complete 360-degree rotation of local director is defined as the pitch ($\boldsymbol{P}$). The chiral behavior of CNC assembly has a strong relevance to the surface charge, aspect ratio, stiffness of crystal and solvent condition [3]. The phase transformation of CNC suspensions occurs spontaneously by evaporation-induced self-assembly (EISA). The wavelength of peak reflected light, λ_{max}, depends strongly on the average refractive index of the local helical structure (n_{av}), pitch ($\boldsymbol{P}$) and the angle φ of incident light with respect to the helical axis [4]. The relationship between these factors can be expressed as:

$$\lambda_{max} = n_{av} \cdot \boldsymbol{P} \cdot \cos\varphi \quad (1)$$

where n_{av} is governed by the CNC specific characteristics including crystallinity, transparency and purity. The pitch $\boldsymbol{P}$ is driven by the suspension interactions and is therefore correlated to the composition of the suspension (the ionic strength of any presence of electrolytes), additives (polymers, surfactants), the surface chemistry of the CNC as well as the drying conditions [5]. The structural color of the dried film can be manipulated to reflect light from the near infrared to the ultraviolet wavelength region.

The structural color created by the CN* phase of CNC has the advantages of good brightness, high saturation, low thermal degradation, and long lifetimes. Such CNC films can also absorb water vapor and swell the CN* structure leading to "red-shift" in the structural color by affecting $\boldsymbol{P}$ dimension [6]. Humidity sensing was identified as a promising application for CNCs [7]. However, it remains difficult to use CNCs alone to produce reliable humidity sensors [8], when compared to other known colorimetric indicator device applied in pesticide control which are based on chemiluminescence assay or phosphorescence [9,10]. One of the major challenges is that CNCs intrinsically possess a low water–adsorption capability, even though they are hydrophilic [11]. The swelling ratio of the CN* structure itself is limited because of the low amount of water entering the structure, which largely resides on the outer surface [12]. Another challenge is highly brittleness of pristine CNC films which is problematic for many practical applications. Researchers have incorporated hygroscopic solvents such as glycerol [13], *N*-Methylmorpholine *N*-Oxide [11] and polymer such as polyethylene glycol (PEG) [14], poly-(3,3′-benzophenone-4,4′-dicarboxylic acid dicarboxylate polyethylene glycol) ester [15], waterborne polyurethane [16] to overcome these problems. Homogeneously distributing these materials into the CN* structure can mediate the internal stress, prevent crack formation [17], and increase film flexibility [18]. The hygroscopicity of these materials enhance the water uptake and encourage larger color shifts.

Specific ion effects (SIE), which encompasses the Hofmeister series named after Franz Hofmeister, are grouped into salting-in and salting-out based on the ions' impact on the precipitation of protein and polymer [19,20]. Salting-in effects solubilize polymer while salting-out effects precipitate polymer. The ions summarized in the Hofmeister series are found to modify the configurations of polymer which generally contain polar and non-polar sections of the polymer chains [19]. Salting-out type ions can increase the polymer structural order and render the macromolecular chains more hydrophobic, so the polymer chains collapse into a dehydrated coil which can precipitate out [21–27]. Salting-in type ions tend to unfold and disorder the chains [24,28] and are usually weakly hydrated and reside toward the center of macromolecular chains [29]. As chains are more hydrophilic, they become more hydrated and swollen [30,31]. SIE have been shown to effectively impact the cloud point of PEG where salting-out type ions reduce the cloud-point temperature [32–35]. In other words, the salting-out type ions change the conformation of PEG chains. This type of ions is usually strongly hydrated and fully shed hydration shells which exclude the hydrophobic section on the polymer chains [36–38]. This action causes the hydrophobic assembly of chains, similar to "aggregation" and creates a secondary phase in aqueous solution with decreasing temperature. Since PEG is commonly intercalated into CN* structure to change the color of dried film [14,39–41], distribution and structure of the polymer within CNC arrangements will determine the brightness and homogeneity of color. Based on our previous study [42], 900,000 Dalton (Da) PEG was selected for better color distribution than lower molecular weight (MW) PEG samples. For lower MW (i.e.20,000 Da PEG), the color from center to edge of a flat dried film is relatively inhomogeneous. The other advantage of choosing this higher MW is to avoid any potential phase separation which may interfere with determining the impact of salts.

In this study, several inorganic salts are selected to have an impact on PEG configuration. Ten ions were chosen based on the order of salting-out and salting-in as illustrated in Fig. 1 and were incorporated into the CNC/PEG composites. To further determine the SIE, the CNC/PEG/Salt suspensions were dried into solid films and then exposed to various levels of relative humidity (RH). The interaction in these ternary systems when they were in suspensions and dried films were characterized. The reflected wavelength

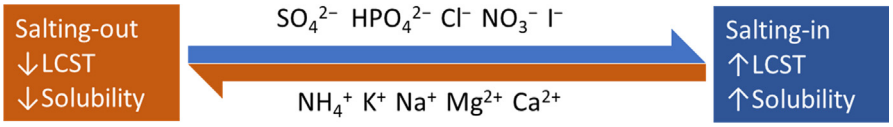

Fig. 1. Ions from conventional Hofmeister series used in this study. Ions on the right side produce a salting-in effect (increasing cloud point and solubility) on the polymer whereas the ions on the left side to a salting out effect.

and the mass of the film were separately monitored in a RH cycle. In the structural analysis, we hypothesized that salt, which changes PEG and CNC conformation during the drying process could alter optical properties. Salts changed the initial color of the solid dried film, as well as the amount of absorbed water, leading to different wavelengths of reflection from 30% RH to 90% RH environment. We found that the performance of color change in response to a changing environment is nearly constant after a month of RH% loop cycling (30%-90%-30%) where the RH was altered daily. We also propose that the ternary system CNC/PEG/salt composite system is promising for colorimetric humidity sensing based on changeable color range and long-term performance.

2. Methods

2.1. Material

CNC samples were purchased from the Maine University Process Development Centre (University of Maine, USA) and had been extracted from wood pulp using sulfuric acid hydrolysis. The original CNC suspension was 10.3 wt% CNC containing 1.1 wt% sulfur with sodium (Na^+) counterions. A commercial PEG was used (Dow Chemicals) with a molecular weight (MW) average of 900,000 Da MW, as defined by the company. The molar mass was also verified by size exclusion chromatography and has been included in the Supporting Information (SI) (Table S1). The inorganic salts in 99.99% trace metals basis, NaCl, KCl, NH_4Cl, $MgCl_2$, $CaCl_2$, NaI, $NaNO_3$, Na_2HPO_4 and Na_2SO_4 were obtained from Sigma-Aldrich and used as received.

2.2. Preparation of CNC composite suspensions and solid films

Aqueous solutions of PEG were prepared by dissolving the relevant amount of the PEG powder in deionized water. The purchased CNC suspension was diluted by the addition of Milli-Q water and stirred for 24 h. Milli-Q water with a resistivity of 18.2 MΩ·cm was used. The CNC suspension and PEG aqueous solution were separately poured into Fisherbrand® dialysis tubing with a 12,000 Da molecular weight cut off (MWCO) and dialyzed with Milli-Q water to remove remnant ions. The water for dialysis was changed every 24 h and the dialysis lasted one month. To prevent potential aggregation of the CNCs after adding electrolyte, the purified CNC suspension and PEG solution were premixed at a specific ratio (m_{CNC}:m_{PEG} = 7:3) and vigorously stirred 48 h at room temperature. Both the ratio and the molecular weight of PEG are the outcome of our previous optimization [42]. This combination of selected ratio and MW was chosen to minimize the depletion interaction of PEG solute between CNC particles and maximize the PEG concentration, in order to increase humidity response. The inorganic salts chosen were dissolved in Milli-Q water to form electrolyte solutions of 5 mM concentrations. 1 mL of electrolyte was added into 10 mL CNC/PEG premixture and incubated in an Infors HT Ecotron incubator (25 °C, 150 rpm) for 24 h. 5 mL volume of each mixture were then cast in petri dishes (d = 35 mm), and the solvent evaporated in a controlled environment (25 °C, 30% RH). In the final dried films, the salt concentration was 50 μmol/g_{CNC}. The remaining suspensions were characterized by Small-Angle X-ray Scattering (SAXS). The mixture is described by the following nomenclature: CNC/PEG/Salt. For example, a CNC and PEG mixture NaCl incorporated is labelled as CNC/PEG/NaCl.

2.3. Characterizations of mixture

2.3.1. Liquid samples

Small angle X-ray scattering (SAXS) characterization was carried out to obtain mesoscopic configuration information in suspension and after water evaporation. Suspension samples were measured at the SAXS/WAXS beamline of the Australian Synchrotron. The suspensions were filled into 1.5 mm thick quartz capillaries and measured in transmission mode at an X-ray energy of 12 KeV. A Pilatus detector with the pixel size of 70 μm × 70 μm was used to collect the scattered X-rays. Glassy carbon and silver behenate were used to calibrate the scattering curves to the absolute units and scaling the q values. The data reduction and averaging of the scattering images was performed using the in-house software Scatterbrain.

2.3.2. Solid samples

Solid dried films were peeled from the base of the petri dish. The cross-sectional images of the thin films were prepared via cryo-fracturing and imaged by a FEI Magellan 400 FEGSEM. The photonic properties of the film were characterized by a Reflectance Spectrometer using an Ocean Optics HDX spectrometer with a DH-2000-L light source (200 nm – 1000 nm) and a UV-NIR reflection probe (six illuminating fibers and one d = 400 μm read fiber), with every sample measured five times across its surface. The information of particle alignment was achieved using lab-based Bruker N8 Horizons SAXS system equipped with a Cu-anode (wavelength = 1.5406 Å) radiation source, Vantec-500 2D detector and Montel multilayer optics. The operating power for the measurement in the transmission mode was 1 kW (KW). The measurement was carried out under vacuum at room temperature. The data processing and analyses were performed using a Bruker DIFFRAC.SAXS program. (Scheme 1).

2.4. Humidity response of CNC based composite films

The water uptake experiment was carried out in the humidity chamber of Cisorp Water Sorption analyzer (CI Electronics) under different control relative humidity (RH) points, 30%, 50%, 70%, 90% where the films were cut into an appropriate size and weighed. The film measurement was completed for every RH point when the amount of water was equilibrated with time. The photonic properties of film were measured by the same Reflectance Spectrometer as described above immediately after the extraction from the humidity chamber and the optical images captured by a digital single lens reflex (DSLR) camera (Sony a6500). At least 5 slices from each film were tested and results are reported as a mean value with standard deviation.

3. Results

A key aim of this research is to elucidate the effect of the type of salt added to the system, whilst the CNC and PEG concentrations

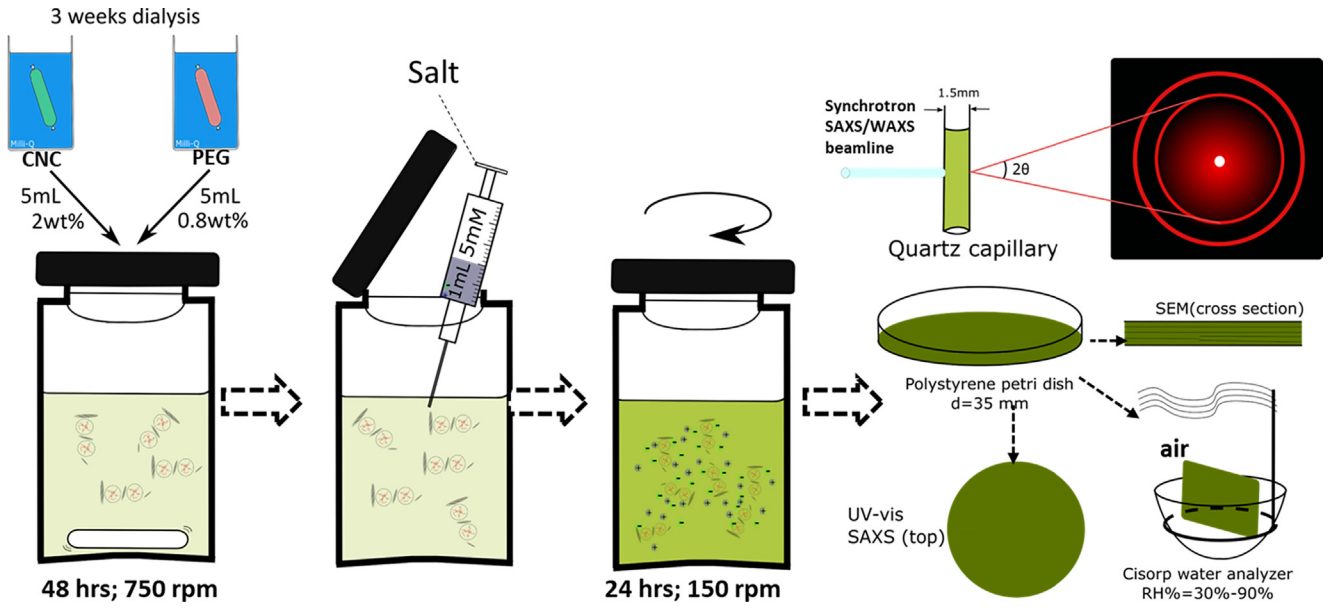

Scheme 1. The process of film production, from pretreating base materials to stirring and incubating before characterizations by SAXS, SEM, UV-NIR measurement, and water analyzer.

were kept constant. The interactions in the ternary system of CNC, PEG and inorganic salts, were investigated using SAXS, SEM and UV-NIR spectroscopy techniques as shown in Scheme.1. The dried films were exposed to water vapor at different relative humidity (RH) in terms of equilibrium and cyclic RH. The weight gain/loss and the color change of films were monitored to examine the impact of the ions on these properties.

3.1. Structure of CNC-based suspensions and their dried films

The structural properties of CNC based suspensions (m_{CNC}(%) = 4-wt%) were characterized by SAXS. The intensity vs q ($Å^{-1}$) SAXS and its Kratky plot are shown in Fig. 2(a-b); the latter is necessary to improve data visualization and analysis. In the original plot, fitting the data was difficult because of the volume polydispersity (PD) of the CNC tactoids. The PD of PEG chain length further complicate data fitting. In previous studies [43,44], the peak in the Kratky plot was used to represent the interparticle distance (axis-to-axis), ***d***. A Gaussian model was applied to the Kratky transformations, with the peaks of ten different samples and the outcomes summarized in Fig. 2(c). The structure of the suspensions was analyzed in terms of ion specificity for the salts added. For cations, only the addition of Mg^{2+} reduced the ***d*** of CNC/PEG from 43.7 ± 0.2 nm to 42.1 ± 0.1 nm. The rest of the cations increased the distance between the CNCs, which indicates swelling of the PEG coils. The behavior of the divalent cations is shown in Fig. 2(c), with the stronger salting-in type ions leading to greater values of ***d***. This contrasts with monovalent cations where salting-out ions cause greater values of ***d***. In terms of anions, only the sample with SO_4^{2-} possessed a smaller ***d*** of 42.4 ± 0.3 nm as compared with CNC/PEG sample. In terms of anions, both monovalent and divalent anions show that the use of the salting-in effect leads to a higher value of ***d***.

The cross-sectional morphology of CNC-based composite films was investigated using SEM. A bar chart presenting all the pitch values of CNC/PEG/salt samples is shown in Fig. 2(f). Other than the CNC/PEG/NaI system, all composite films with salts have a smaller pitch size than the control group. Furthermore, the standard deviations (SD) of the composites which contain a salt are smaller than those without. For example, the SD of CNC/PEG/KCl value of ***d*** is 20.9 nm, while the SD without ions is 73.7 nm., The smallest pitch size of all CNC composites and cation types is shown in Fig. 2(f) and is 192.7 nm for films with Mg^2. The comparison between Mg^{2+} and Ca^{2+} indicates an underlying relationship between the salting-in type ions and the magnitude of the pitch.

For CNC composites containing monovalent cations, there is no clear pattern of pitch dimensions related to their salting-in or salting-out nature. In comparison, the pitch sizes of both monovalent and divalent anions follow the relationship in which the stronger salting-in effect demonstrate a larger pitch size, in accordance with the values of ***d*** found by SAXS measurement of suspension. The largest pitch size is found in the CNC/PEG/NaI film (Fig. 2(e)). The addition of salt increases the definition of each layer (sharper peak), which allows for a better determination of pitch size, and also contributing to a reduced value of SD, as determined from the SEM images in Fig. 2(d-e) and Fig. S1 in SI.

3.2. Humidity response of CNC based films

3.2.1. Color changes as increases RH

The change in iridescence of the colorful films by addition of different ions is shown in Fig. 3. Each film was exposed to four levels of RH (30%, 50%, 70% and 90%) to measure changes in term of the dominant wavelength polarized (λ_{max}) and moisture content. The "red cross" symbols in Fig. 3 indicate there was no measurable λ_{max}, as the maximum measurable wavelength that can be measured by our instrument is 1100 nm. Examples of such spectra are presented in Fig. S2. The increments of wavelength ($\Delta\lambda$) in Fig. 3(b, e) are calculated from the difference between two neighboring λ_{max} based on Fig. 3(a, d), such as $\Delta\lambda$(30%-50%) = λ_{max} (50%) - λ_{max} (30%). As all films were equilibrated in a high humid environment, λ_{max} values are beyond the human visible spectrum. For films containing salts, $\Delta\lambda$ is larger at higher relative humidity compared to the control group.

Examining the cations reveals the upward trend lines of λ_{max} changed similarly for all systems as the RH was increased from 30% to 90%. At 30% RH, the highest recorded wavelength was when Na^+ was included and resulted in a red film with a value of 720.2 ± 4.8 nm. Conversely, the minimum recorded wavelength was achieved with the addition of Ca^{2+} which led to a yellow green film

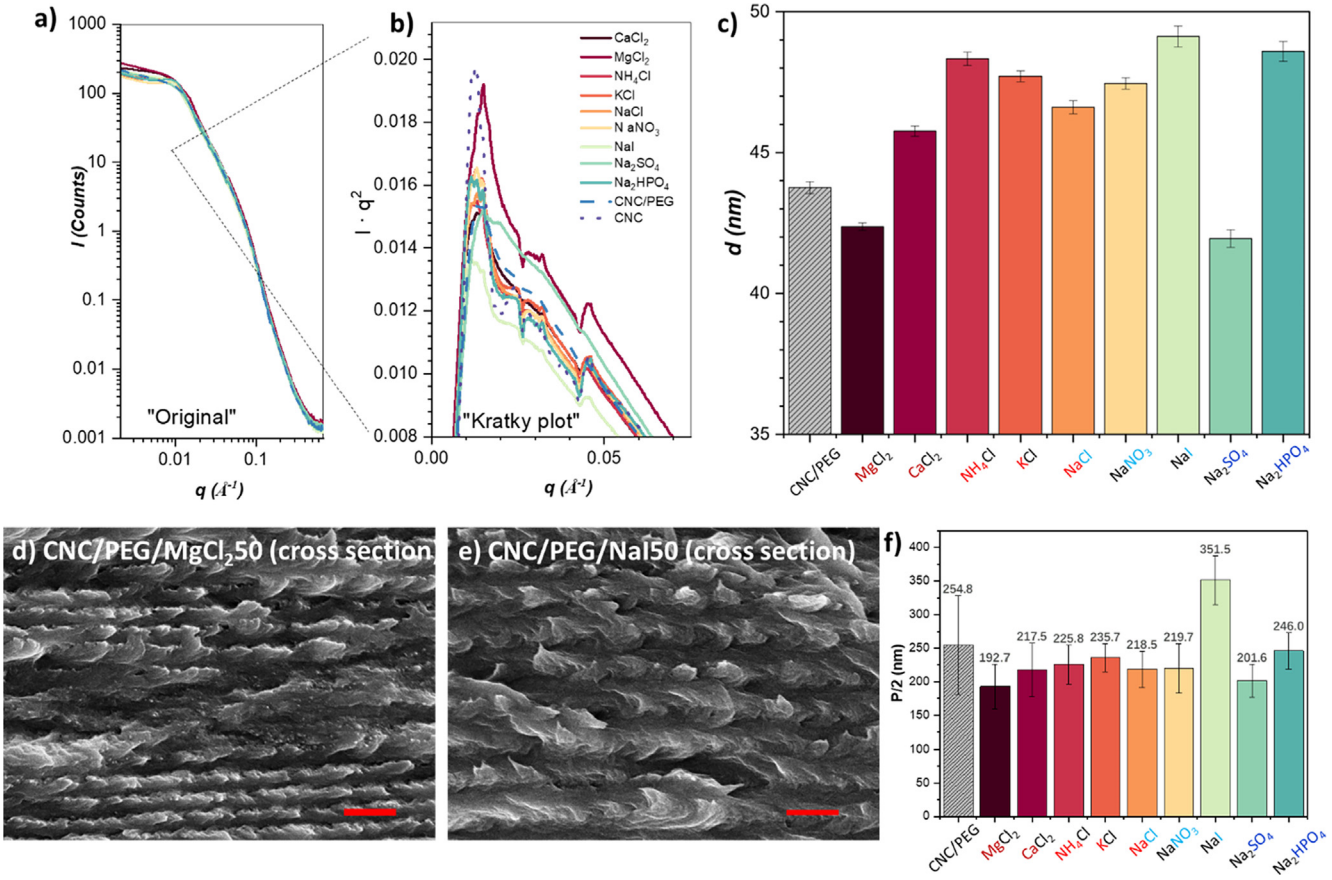

Fig. 2. The outcome of structural characterizations for producing CNC based humidity sensitive film. The original plot (a) in Log_{10} scale and Kratky plot (b) in linear scale of SAXS measurements of liquid CNC/PEG/Salt composites, where CNC is 4.0 wt%, PEG is 1.7 wt% and salt concentration is 50 $\mu mol/g_{CNC}$. (c) is the summary of axis-to-axis interparticle distance, ***d***, of composite systems for 9 different types of salt plus a control group (CNC/PEG). (d-e) are the SEM images of CNC/PEG/$MgCl_2$ and CNC/PEG/NaI showing the significant difference in pitch size with the 500 nm scale bar. (f) is the summary of measured half-pitch (***P***/2) size by ImageJ software.

with a wavelength of 585.2 ± 5.4 nm. With increasing RH, the trend was maintained with the $\Delta\lambda$ of the Na^+ film being the largest, and $\Delta\lambda$ of the Ca^{2+} film being the smallest. The trend for $\Delta\lambda$ as a function of salting-in effect was not found to be consistent with ion valency. Divalent cations behave differently from monovalent species. For example, Ca^{2+} has stronger salting-in effect than Mg^{2+} but $\Delta\lambda$ s for Ca^{2+} film and Mg^{2+} film are close, especially considering the SD. In contrast, for monovalent systems, salting-in type cations such as NH_4^+ have a larger $\Delta\lambda$ with RH change. Thus, the impact of cations on CNC films optical and water–vapor-adsorption properties is not only affected by their salting-in properties, but also by their valences.

The values of λ_{max} for CNC films with all types of anions show increase over the full RH range (30% –90%), as shown in Fig. 3(d, e). At 30% RH, CNC films with lower ionic strength exhibit a larger λ_{max} as the films undergo a red shift. Films containing, I^- and SO_4^{2-} ions demonstrate the largest and the lowest λ_{max}, respectively (Fig. 3(f)). Focusing on the salting-in variation of the ions, the HPO_4^{2-} film is redder than the SO_4^{2-} film over the whole RH range measured. I^- films exhibit the deepest red or the highest wavelength among the monovalent anions systems (Cl^-, NO_3^-, I^-) from 30% to 70%. Furthermore, the trend of $\Delta\lambda$ as a function of salting-in effect is consistent with the valences. For example, $\Delta\lambda_{30\%-90\%}$ of the NO_3^- film is larger than that for the films with Cl^- ions. Meanwhile, the HPO_4^{2-} film shows a greater $\Delta\lambda_{30\%-90\%}$ than the SO_4^{2-} films. In summary, salting-in type anions play an important role in controlling color changes in these CNC/PEG/Ion ternary composite films (Fig. 3(d-f)).

3.2.2. Mass changes (Δm (%)) as function of RH

The effect of relative humidity on the CNC films water absorption and its effect on color change was quantified. The original curves recording the mass during a RH cycle are normalized and presented in Fig. 4(a-b). In addition to change in mass, we define a mass response rate of a film ($\frac{\partial m(\%)}{\partial t}$) to describe how sensitive the color/wavelength is to the uptake of water. The outcomes of these calculations are summarized in Fig. 4(c-e).

Changes in water uptake in the highest RH range (70%-90%) lead to the strongest changes. When RH increased from 30% – 50 or decreased from 50% – 30%, the changes are lower. Comparing the upper and lower part of Fig. 4(a-b) reveals no measurable difference in mass change of the same RH range during humidification and dehumidification. This phenomenon shows good reversibility, as there is little hysteresis of these CNC-based humidity sensors. All CNC/PEG/salt films demonstrate a larger mass change than the control system (CNC/PEG, no salt). Inconsistent trends of mass change as a function of RH are found between monovalent and divalent cations. For example, the weight of Ca^{2+} film increased to 31.4% while Mg^{2+} film only icreased by 27.7% weight (Fig. 4(a)). salting-in type divalent cations could be expected to have higher water adsorption. However, Na^+ ions, the most salting-in type of monovalent cations in the present study, demonstrates the least mass gain, only increasing up to 27.75%. In contrast, the trends of monovalent anions agree with those of divalent anions, although the differences are small for both valences. For example, the difference between NO_3^- and I^- is only 0.20 %.

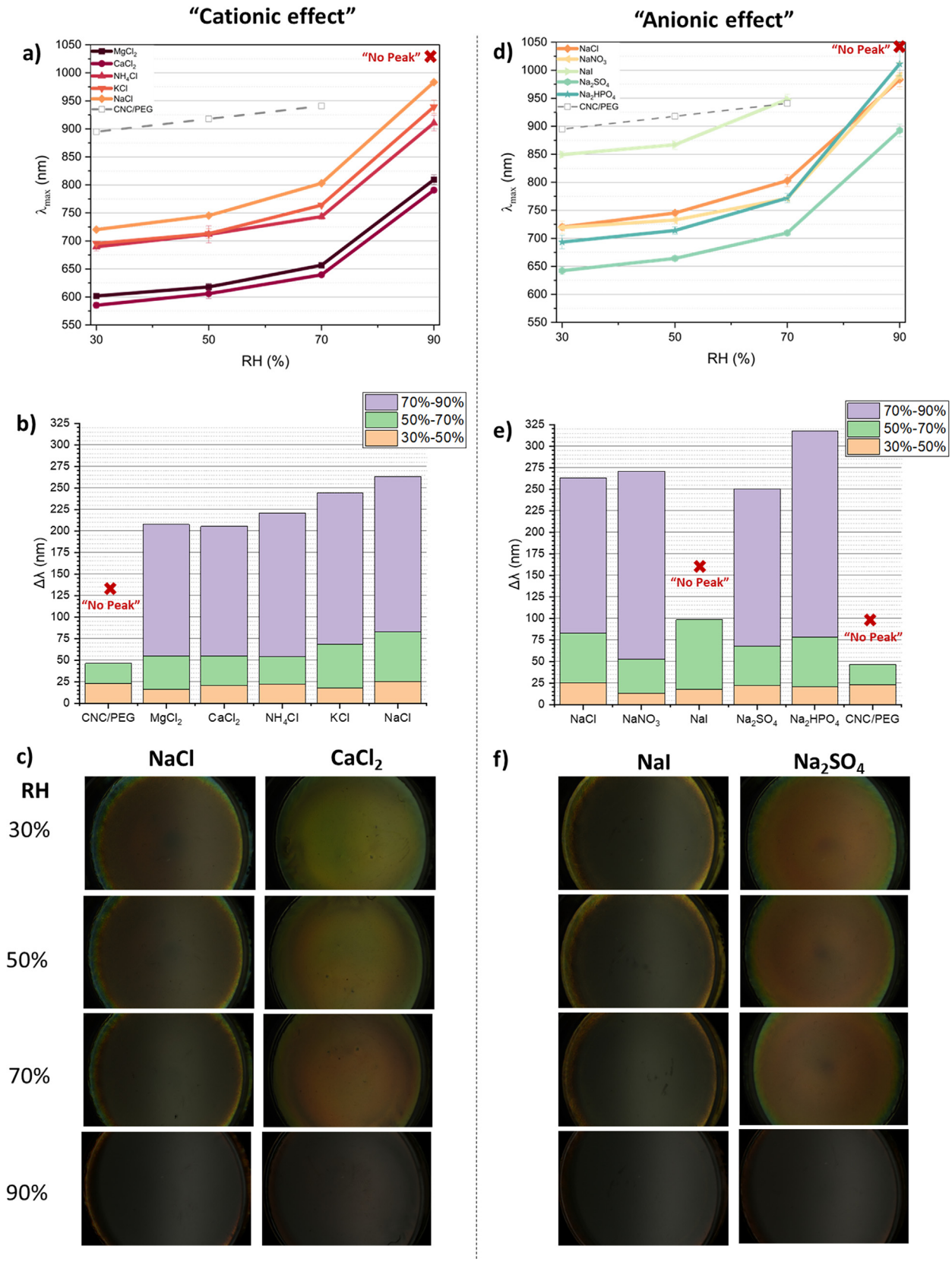

Fig. 3. The impact of the type of cations (a-c) and anions (d-f) on photonic properties of CNC/PEG/Salt composite films. (a, d) are the change in wavelength of reflected light as a function of environmental humidity. (b, e) are the increment/decrement of wavelength change in the range of RH%. (c, f) are representative photos showing the impact of cations and anions on photonic properties. (a, d) are the wavelength of reflected light changes with environmental humidity. (b, e) are the increment/decrement of wavelength change as a function of RH%. (c, f) are the visual images of CNC/PEG/NaI, CNC/PEG/$MgCl_2$.

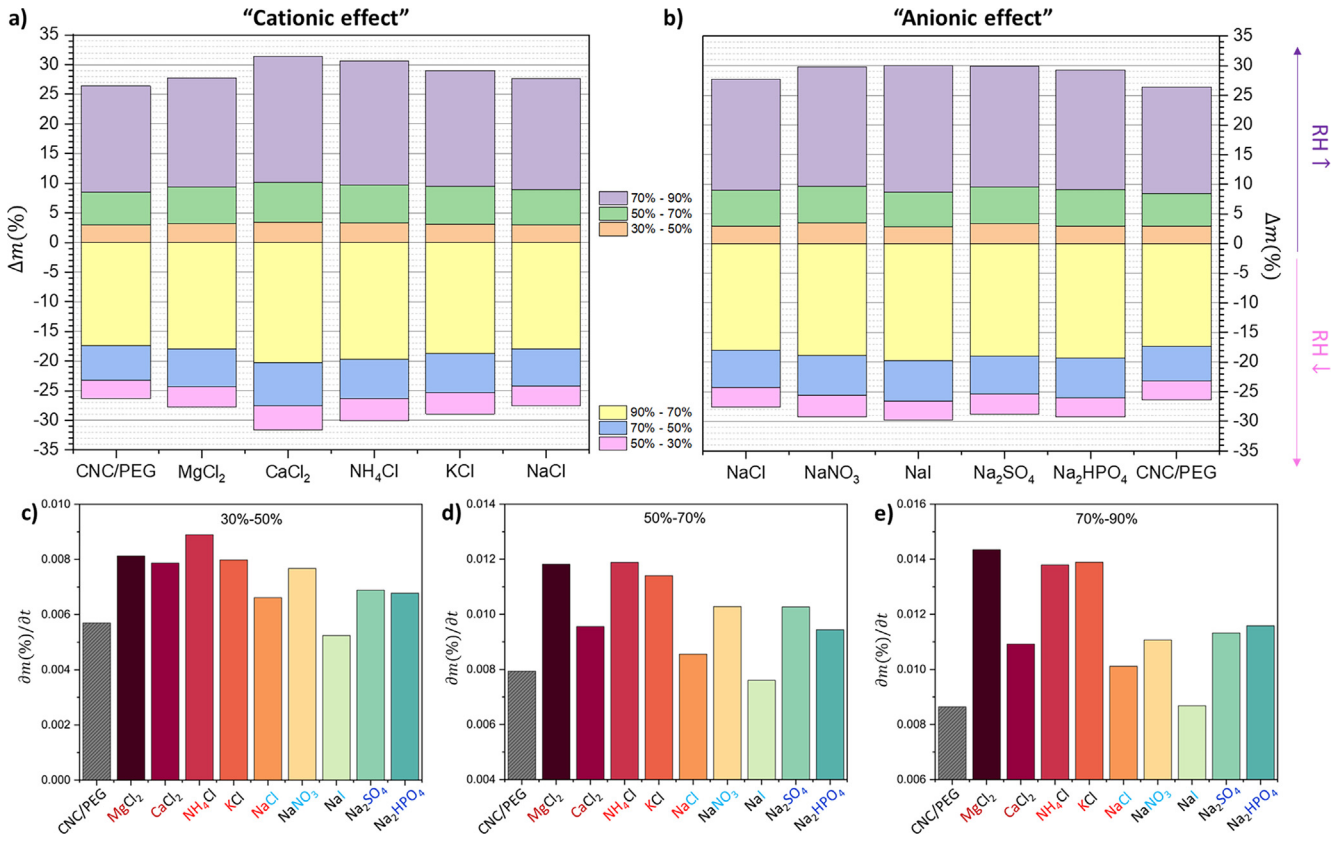

Fig. 4. The impact of (a,c) cations and (b,d) anions on water adsorption/desorption properties of CNC/PEG/Salt films. (a,b) the mass changes in a cycle of RH increase followed by decrease. (c-e) summarize the peak values of first derivative of a function of mass change related to time ($\frac{\partial m(\%)}{\partial t}$) in three RH range, 30%-50%, 50%-70% and 70%-90% from Fig. S4 in SI.

The peaks value (derived from the highlighted grey area in Fig. S4) of mass responsive rate in each RH range are summarized in Fig. 4(c-e). In Fig. 4(c), for both divalent and monovalent cations, the sequence of mass response rate follow the anti-Hofmeister series ($Mg^{2+} > Ca^{2+}$, $NH_4^+ > K^+ > Na^+$). In the RH region of 50% – 70% and 70% – 90%, the sequence regarding to peak value remain similar except the one for K^+ film surpassing that for NH_4^+ film. For the group of anions, all peak heights at each specific RH region are lower than that of cations. For the group of anions, there is a strongly indicated sequence regarding to peak value ($SO_4^{2-} \approx HPO_4^{2-} \approx NO_3^- > Cl^- > I^- >$ Control) from all RH range. These sequences for cations and anions neither match their order in the Hofmeister series nor the values of ΔM. If ΔM is closely related to the salting-in and salting-out impacts on CNC/PEG arrangement, mass response rate may further involve the outer surface topology of films such as porosity.

3.2.3. Performance after multiple humidity cycles

The long-term performance of the CNC-based films was studied to understand if the structural integrity and functionality remain after 30 cycles of water adsorption - desorption. The color and mass of the films were constantly measured in RH cycles, 30%-90%-30%-90%. In Fig. 5, the CNC/PEG/$MgCl_2$ system is used as an example to represent changes in weight and wavelength after varying humidity. A complete set of data is presented in Table S1. From Fig. 5(a), λ_{max} at 30% deviated by less than 4 nm, while the change increased to 14–30 nm after cycling at 90%. From Table S1, only CNC/PEG/Na_2SO_4 and CNC/PEG/NH_4Cl are both stable at two RH points (30% and 90%). Other films such as CNC/PEG/$CaCl_2$, CNC/PEG/KCl and CNC/PEG/NaCl have a blue-shift color at 90% compared to the first loop, while the CNC/PEG/Na_2HPO_4 and CNC/PEG/NaI show a red-shift color at 30%. The mass of the films is relatively stable, and the difference between maxima and minima in the scan cycle is less than 1%, even after 30 cycles.

4. Discussion

From the measurement of structure to the quantification of performance, the difference of the color, color range and mass increment do not follow the order of salting-in type cations but follow the order of salting-in type anions. Stronger salting-in effect can offer larger color range, accompanied with larger mass increment as RH increases. Such a correlation is not present in cations group. Furthermore, trends of salting-in type cations are not dependent on valences, whilst the trends of the anions are. In terms of Hofmeister effect on controlling the pitch size, the effect of anions is more significant than that of the cations. However, before comparing the cationic and anionic influence on the performance of dried films regarding to RH the nature of two interactions: the one between salt and CNC, and the second between salt and PEG need to be analyzed.

4.1. Specific ion effect is present in CNC systems

To determine if SIE is occurring and governing behavior in CNC based systems, a comparison between previous studies on CNC systems and our work is necessary. Cao et al. [45] and Xu et al. [43] concluded that ions affecting the colloidal stability of sulfated CNC follow the similar sequence as those summarized in Hofmeister series. In Cao et als work [45], monovalent cations, those which were more salting-in, led to higher critical coagulation concentra-

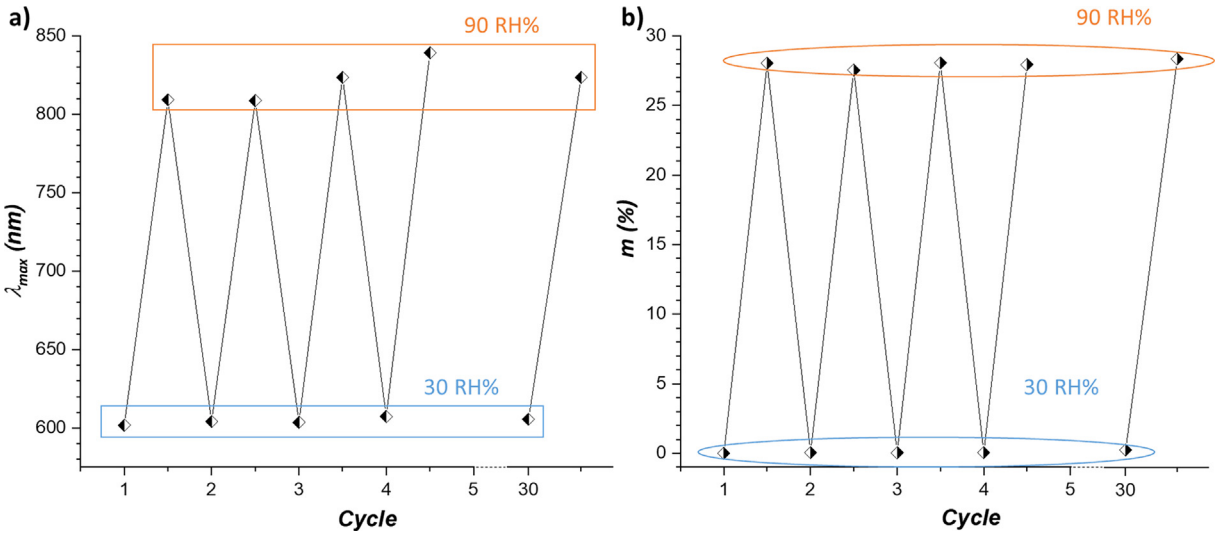

Fig. 5. The long-term performance of CNC based films in two separate cyclic measurements - (a) λ_{max} and (b) m (%) during 30 cycles.

tions (CCC); the trend was opposite for divalent cations. However, Metzger et al [46] found the cations do not follow the Hofmeister series in critical aggregation concentration, especially for the monovalent cations. While Cao et al. [45] considered the ion adsorption efficiency on the surface of CNC particles, Metzger et al. theorized that the stability can be attributed to electrostatic charge screening, CNC cluster formation and the affinity between sulfate groups and ions. In other cellulose system, Barajas-Ledesma and co-workers [47] found that the swelling ratio of TEMPO-oxidized cellulose nanofiber gel was connected to SIE, where it was found that salting-in cations resulted in less water adsorption for fiber network. It was claimed that SIE of cations was not only related to the electrostatic interaction between the functional groups on cellulose surface and cations, but also the hydrophilicity of cellulose, or maybe even the inner structure of cellulose [47]. Comparing these three previous studies confirms that the relationship between salting-in type cations and CNC has not been satisfactory defined yet. Anions, on the other hand, have been less studied in CNC systems. Xu et al [43] concluded that NaSCN has a higher critical coagulation concentration than NaCl which has less potential to destabilize colloidal stability of CNC. The observation is in agreement with theory, as SCN^- is a larger anion.

In our system, an additional set which only include dialyzed CNC and salts is investigated and utilized as a baseline for CNC/PEG/Salt system. Interparticle distance indirectly show the interaction between electrolytes and CNC particles. The difference of interparticle distance between salt containing systems and control groups are expressed as $\Delta \boldsymbol{d}_{CNC/PEG/Salt}$ in Fig. 6(a) and $\Delta \boldsymbol{d}_{CNC/Salt}$ in Fig. 6(b) to better illustrate salt impact. $\Delta \boldsymbol{d}_{CNC/PEG/Salt}$ and $\Delta \boldsymbol{d}_{CNC/Salt}$ can be calculated by.

$$\Delta \boldsymbol{d}_{CNC/PEG/Salt} = \boldsymbol{d}_{CNC/PEG/Salt} - \boldsymbol{d}_{CNC/PEG} \quad (2)$$

$$\Delta \boldsymbol{d}_{CNC/Salt} = \boldsymbol{d}_{CNC/Salt} - \boldsymbol{d}_{CNC} \quad (3)$$

where $\boldsymbol{d}_{CNC/PEG/Salt}$, $\boldsymbol{d}_{CNC/PEG}$, $\boldsymbol{d}_{CNC/Salt}$ and $\boldsymbol{d}_{CNC}$ are the interparticle distances of CNC/PEG/Salt, CNC/PEG, CNC/Salt and pristine CNC suspension from SAXS measurement. There are two major factors controlling the scale of $\boldsymbol{d}$: the conformation of PEG and the Debye length of CNC. The Debye length decreases as an electrolyte is added due to charge screening. Given the same concentration for all salts, different eventual ionic strengths for monovalent and divalent ions due to stoichiometry makes these two types incomparable for any potential SIE. For non-PEG system in Fig. 6(b), shorter $\Delta \boldsymbol{d}_{CNC/Salt}$ indicates more aggressive interaction. SIE exists in CNC aqueous suspension and demonstrates itself by the different magnitude of electrostatic interaction. In CNC/PEG/Salt ternary system, in addition to the two standalone interactions (i.e., CNC-ions and PEG-ion), there is a competition between CNC and PEG that either of them tries to bind more ions than the other. Based on studies from Ataman [32,33], the salting-in and salting-out effect based on Hofmeister series have been observed in aqueous PEG solutions. The salting-in effect increases PEG solubility in water and its cloud point as temperature increases, whilst the salting-out effect ends up with a phase separation between PEG and water and a decrease in its cloud point. Due to the sequence of mixing, PEG was firstly intercalated between CNC particles. In Fig. 6(a), the addition of PEG before salt was added also reduced the ability of the electrolytes to screen the charges of CNCs. Neither $MgCl_2$ nor Na_2SO_4 decreases $\boldsymbol{d}_{CNC/PEG}$ as they do in CNC/Salt system. The addition of rest of salts in our system even expands $\boldsymbol{d}_{CNC/PEG}$. Supposedly, the added salting-in type ions can penetrate PEG coils and have more contact with the inner PEG chain sequences, instead of the surface of CNC particles where such schematic is shown in Fig. 6(c). PEG coils then swell to a greater volume with increasing humidity. However, for the monovalent cations, ions with less salting-in effect cause larger $\Delta \boldsymbol{d}_{CNC/PEG/Salt}$ than those with a stronger salting-in effect. Such a phenomenon is likely induced by more numbers of Na^+ ions preferably binding with CNC than NH_4^+ and K^+ ions.

When these suspensions were dried to a solid film, their interparticle distance (Fig.S5) and pitch size (Fig. 2(f)) remain smaller than in a CNC/PEG film. During the loss of water, contacts between CNC particles and salts occur more frequently, and the ionic strength of solvent increases. Arguably, as ion concentration [48,49] changes within aqueous electrolytes, the SIE can deviate from the order of ions in a conventional Hofmeister series. However, within our experimental errors, the sequence of SIE in dried films remains similar to that in suspension based on the comparison of Fig. 2(c) and (f).

4.2. The manipulation of water adsorption

Understanding how water molecules interact with the nanostructures of iridescent film is crucial to manipulate water-uptake capability and tailor the humidity response of colorimetric humid-

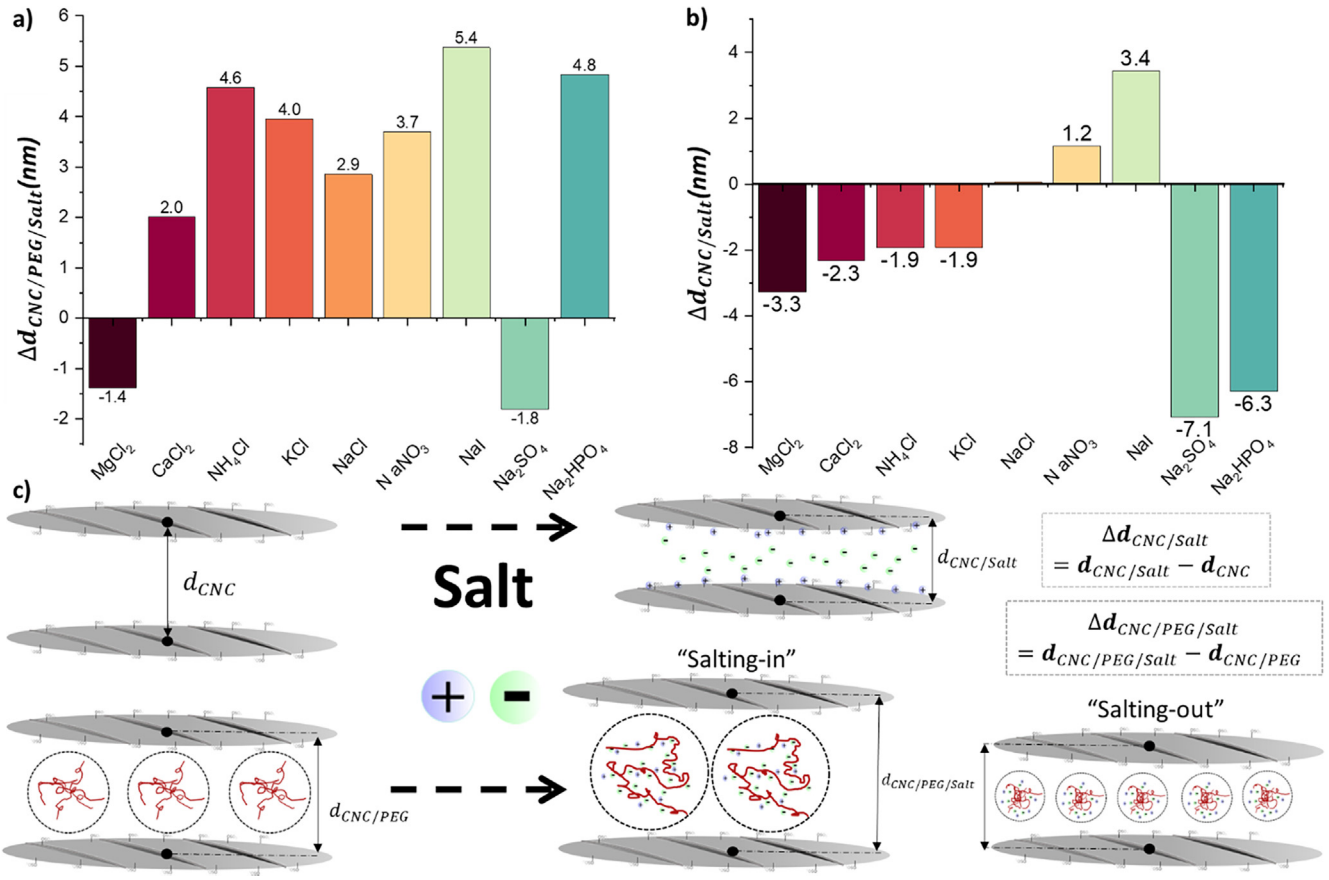

Fig. 6. The salt impacts on two neighbor CNC particles in different systems with the same concentration. a) the difference between before and after adding the salts in CNC/PEG system. b) the difference between before and after adding the salts in CNC system. c) the schematic representation of which salts impact CNC and CNC/PEG system.

ity sensors. By comparing Fig. 3(b, e) and Fig. S6(c-d), the addition of PEG is essential to increase the rate in wavelength change as a function of changing humidity. PEG acts as a spacer between CNC particles and becomes swollen after attracting water molecules because of its hydrophilic characteristics. The conformation of intercalation was retained after drying. From our results, salting-in type anions cause larger pitch size, λ_{max}, $\Delta\lambda$ and mass change. Since both hydroxyl groups at the end of PEG chain and ether oxygen [50] at the middle of PEG chains dictate water affinity of the chains, when the dried films were in contact with water vapor, the open PEG chains have more moieties exposed to humid air. If the anions demonstrate an increased salting-out effect, PEG chains are packed more densely during the film making process. Only the outer part of packed coils can interact with water molecules, leading to a smaller increase in volume. Due to the correlation between pitch size and λ_{max}, the salting-out effect eventually results in a reduced Δ.

The long-term performance of these materials measured by cyclic RH variation is consistent for all the cationic and anionic systems. CNC/PEG films show a stable long-term performance, showing that the volume of PEG coils can be reversibly changed. The addition of salts in this work does not compromise this property. The reason for seeing a minor blue or red shift of color after a few cycles may be due to the rearrangement of PEG coils when films absorb enough water. At a high humidity, such a packed structure of CNC and PEG may be loosened. Fig. 5(b), where mass values at 30% RH and 90% RH are almost constant, indicating that the PEG conformation did not change during the humidity cycling tests.

5. Conclusion

The optical (color) and water absorption properties of CNC/PEG films were manipulated by the addition five types of inorganic anions mirroring the order of Hofmeister series. By combining SAXS and SEM analysis of these mixtures based on the previously reported preparative approaches [5,14,42,45], the structure of the aqueous CNC suspensions and their subsequent solid dried films showed that the addition of anions impacts the PEG spacer that sits between CNCs and modifies the electrostatic interactions due to the surface charge of the CNC particles. However, it is found that series of anions and cations affect the system differently. No clear and consistent relationship related the properties of the cellulosic films as a function of the cation type mirroring the order of Hofmeister series; this differs from some previous studies [43,45,46]. Anions affect the color and absorption behaviors of CNC/PEG/salt films. The order of salting-in anions in this study matches with previous studies which focused on the impact on critical coagulation concentration [32,33,43]. The trend for the anions on the CNC film properties was the same for both monovalent ($Cl^- < NO_3^- < I^-$) and divalent ($SO_4^{2-} < HPO_4^{2-}$) ions. Salting-in type ions resulted in a greater spacer between CNC particles by virtue of their increasing the volume of PEG and weakening electrostatic interactions between particles. These behaviors are consistent with the Hofmeister effect on the colloidal stability of nanocellulose, as previously reported [43]. The addition of I^- and HPO_4^{2-} ions induced the highest λ_{max}, the largest $\Delta\lambda$ and the maximum water absorption. The mass response rates (water uptake rates) of all CNC films are similar and their long-term performance over a month was broadly stable. The variation of the PEG chain conformation is

believed to be the cause of anion specificity effect based on the Hofmeister series. More salting-in effects result in PEG chains being more extended, rather than being coagulated during film drying. Hydrophilic groups on the chains have a greater chance to bind water molecules from humid air and such an increased water adsorption helps to increase the range of colors accessible. This mechanism allows CNC/PEG/anions films to be used as tailorable, humidity sensors by manipulating the incorporated anions.

CRediT authorship contribution statement

Maoqi Lin: Conceptualization, Methodology, Writing – original draft, Visualization, Formal analysis. **Vikram Singh Raghuwanshi:** Validation, Software, Writing – review & editing, Formal analysis. **Christine Browne:** Validation, Investigation, Writing – review & editing, Formal analysis. **George P. Simon:** Writing – review & editing, Supervision, Project administration, Resources. **Gil Garnier:** Writing – review & editing, Supervision, Project administration, Funding acquisition, Resources.

Declaration of Competing Interest

The authors declare that they have no known competing financial interests or personal relationships that could have appeared to influence the work reported in this paper.

Acknowledgements

This work was funded by the Australian Research Council – Industry Transformation Research Hub; Processing Advanced Lignocellulosic (PALS) [Grant Number IH170100020]. The authors also acknowledge SEM support from Monash Centre for Electron Microscope, Monash University (Clayton). Authors thank to Dr. Nigel Kirby and SAXS/WAXS beamline at Melbourne Synchrotron beamline and support from the Australian Nuclear Science and Technology Organization (ANSTO). Thanks to the Monash X-ray platform, Monash University (Clayton) for SAXS beamline measuring dried films.

Appendix A. Supplementary material

Supplementary data to this article can be found online at https://doi.org/10.1016/j.jcis.2022.09.101.

References

[1] K. Dhali, M. Ghasemlou, F. Daver, P. Cass, B. Adhikari, A review of nanocellulose as a new material towards environmental sustainability, Sci. Total Environ. 775 (2021) 145871.
[2] K.J. Nagarajan, N.R. Ramanujam, M.R. Sanjay, S. Siengchin, B. Surya Rajan, K. Sathick Basha, P. Madhu, G.R. Raghav, A comprehensive review on cellulose nanocrystals and cellulose nanofibers: pretreatment, preparation, and characterization, Polym. Compos. 42 (4) (2021) 1588–1630.
[3] R. Kádár, S. Spirk, T. Nypelö, Cellulose nanocrystal liquid crystal phases: progress and challenges in characterization using rheology coupled to optics, scattering, and spectroscopy, ACS Nano 15 (5) (2021) 7931–7945.
[4] H. De Vries, Rotatory power and other optical properties of certain liquid crystals, Acta Crystallogr. A 4 (3) (1951) 219–226.
[5] R.M. Parker, G. Guidetti, C.A. Williams, T. Zhao, A. Narkevicius, S. Vignolini, B. Frka-Petesic, The self-assembly of cellulose nanocrystals: hierarchical design of visual appearance, Adv. Mater. 30 (19) (2018) 1704477.
[6] G. Zhao, Y. Zhang, S. Zhai, J. Sugiyama, M. Pan, J. Shi, H. Lu, Dual response of photonic films with chiral nematic cellulose nanocrystals: humidity and formaldehyde, ACS Appl. Mater. Interfaces 12 (15) (2020) 17833–17844.
[7] Z. Li, J. Wang, Y. Xu, M. Shen, C. Duan, L. Dai, Y. Ni, Green and sustainable cellulose-derived humidity sensors: a review, Carbohydr. Polym. 270 (2021) 118385.
[8] N. Bumbudsanpharoke, S. Kwon, W. Lee, S. Ko, Optical response of photonic cellulose nanocrystal film for a novel humidity indicator, Int. J. Biol. Macromol. 140 (2019) 91–97.
[9] R. Umapathi, S. Sonwal, M.J. Lee, G. Mohana Rani, E.S. Lee, T.J. Jeon, S.M. Kang, M.H. Oh, Y.S. Huh, Colorimetric based on-site sensing strategies for the rapid detection of pesticides in agricultural foods: New horizons, perspectives, and challenges, Coord. Chem. Rev. 446 (2021) 214061.
[10] R. Umapathi, B. Park, S. Sonwal, G.M. Rani, Y. Cho, Y.S. Huh, Advances in optical-sensing strategies for the on-site detection of pesticides in agricultural foods, Trends Food Sci. Technol. 119 (2022) 69–89.
[11] Y. Zhang, Z. Tian, Y. Fu, Z. Wang, M. Qin, Z. Yuan, Responsive and patterned cellulose nanocrystal films modified by N-methylmorpholine-N-oxide, Carbohydr. Polym. 228 (2020) 115387.
[12] Y.u. Zhang, Z. Tian, Y. Fu, Z. Wang, M. Qin, Z. Yuan, Responsive and patterned cellulose nanocrystal films modified by N-methylmorpholine-N-oxide, Carbohydr. Polym. 228 (2020) 115387.
[13] Y. Meng, Y. Cao, H. Ji, J. Chen, Z. He, Z. Long, C. Dong, Fabrication of environmental humidity-responsive iridescent films with cellulose nanocrystal/polyols, Carbohydr. Polym. 240 (2020) 116281.
[14] K. Yao, Q. Meng, V. Bulone, Q. Zhou, Flexible and responsive chiral nematic cellulose nanocrystal/poly(ethylene glycol) composite films with uniform and tunable structural color, Adv. Mater. (Deerfield Beach Fla.) 29 (28) (2017) 1701323.
[15] H. Chen, A. Hou, C. Zheng, J. Tang, K. Xie, A. Gao, Light- and humidity-responsive chiral nematic photonic crystal films based on cellulose nanocrystals, ACS Appl. Mater. Interfaces 12 (21) (2020) 24505–24511.
[16] Y. Sui, X. Li, W. Chang, H. Wan, W. Li, F. Yang, Z.-Z. Yu, Multi-responsive nanocomposite membranes of cellulose nanocrystals and poly(N-isopropyl acrylamide) with tunable chiral nematic structures, Carbohydr. Polym. 232 (2020) 115778.
[17] M. Kim, K. Pierce, M. Krecker, D. Bukharina, K. Adstedt, D. Nepal, T. Bunning, V. V. Tsukruk, Monolithic chiral nematic organization of cellulose nanocrystals under capillary confinement, ACS Nano 15 (12) (2021) 19418–19429.
[18] P. Liu, X. Guo, F. Nan, Y. Duan, J. Zhang, Modifying mechanical, optical properties and thermal processability of iridescent cellulose nanocrystal films using ionic liquid, ACS Appl. Mater. Interfaces 9 (3) (2017) 3085–3092.
[19] S.Z. Moghaddam, E. Thormann, The Hofmeister series: Specific ion effects in aqueous polymer solutions, J. Colloid Interface Sci. 555 (2019) 615–635.
[20] K.P. Gregory, G.R. Elliott, H. Robertson, A. Kumar, E.J. Wanless, G.B. Webber, V. S.J. Craig, G.G. Andersson, A.J. Page, Understanding specific ion effects and the Hofmeister series, PCCP 24 (21) (2022) 12682–12718.
[21] Y. Zhang, S. Furyk, D.E. Bergbreiter, P.S. Cremer, Specific ion effects on the water solubility of macromolecules: PNIPAM and the Hofmeister series, J. Am. Chem. Soc. 127 (41) (2005) 14505–14510.
[22] J. Heyda, J. Dzubiella, Thermodynamic description of hofmeister effects on the LCST of thermosensitive polymers, J. Phys. Chem. B 118 (37) (2014) 10979–10988.
[23] T.J. Murdoch, B.A. Humphreys, J.D. Willott, K.P. Gregory, S.W. Prescott, A. Nelson, E.J. Wanless, G.B. Webber, Specific anion effects on the internal structure of a poly(N-isopropylacrylamide) brush, Macromolecules 49 (16) (2016) 6050–6060.
[24] T.J. Murdoch, B.A. Humphreys, E.C. Johnson, G.B. Webber, E.J. Wanless, Specific ion effects on thermoresponsive polymer brushes: Comparison to other architectures, J. Colloid Interface Sci. 526 (2018) 429–450.
[25] B.A. Humphreys, E.J. Wanless, G.B. Webber, Effect of ionic strength and salt identity on poly(N-isopropylacrylamide) brush modified colloidal silica particles, J. Colloid Interface Sci. 516 (2018) 153–161.
[26] I. Shechter, O. Ramon, I. Portnaya, Y. Paz, Y.D. Livney, Microcalorimetric study of the effects of a chaotropic salt, KSCN, on the lower critical solution temperature (LCST) of aqueous poly(N-isopropylacrylamide) (PNIPA) solutions, Macromolecules 43 (1) (2010) 480–487.
[27] Y. Zhang, S. Furyk, L.B. Sagle, Y. Cho, D.E. Bergbreiter, P.S. Cremer, Effects of Hofmeister anions on the LCST of PNIPAM as a function of molecular weight, J. Phys. Chem. C 111 (25) (2007) 8916–8924.
[28] T.J. Murdoch, B.A. Humphreys, J.D. Willott, S.W. Prescott, A. Nelson, G.B. Webber, E.J. Wanless, Enhanced specific ion effects in ethylene glycol-based thermoresponsive polymer brushes, J. Colloid Interface Sci. 490 (2017) 869–878.
[29] B.A. Rogers, H.I. Okur, C. Yan, T. Yang, J. Heyda, P.S. Cremer, Weakly hydrated anions bind to polymers but not monomers in aqueous solutions, Nat. Chem. 14 (1) (2022) 40–45.
[30] A. Lendlein, V.P. Shastri, Stimuli-sensitive polymers, Adv. Mater. 22 (31) (2010) 3344–3347.
[31] I.T.S. Li, G.C. Walker, Single polymer studies of hydrophobic hydration, Acc. Chem. Res. 45 (11) (2012) 2011–2021.
[32] M. Ataman, E.A. Boucher, Properties of aqueous salt solutions of poly(ethylene oxide), J. Polym. Sci.: Polym. Phys. Ed. 20 (9) (1982) 1585–1592.
[33] M. Ataman, Properties of aqueous salt solutions of poly(ethylene oxide). Cloud points, θ temperatures, Colloid Polym. Sci. 265 (1) (1987) 19–25.
[34] E.A. Boucher, P.M. Hines, Effects of inorganic salts on the properties of aqueous poly(ethylene oxide) solutions, J. Polym. Sci.: Polym. Phys. Ed. 14 (12) (1976) 2241–2251.
[35] E.A. Boucher, P.M. Hines, Properties of aqueous salt solutions of poly(ethylene oxide): thermodynamic quantities based on viscosity and other measurements, J. Polym. Sci.: Polym. Phys. Ed. 16 (3) (1978) 501–511.
[36] W.F. McDevit, F.A. Long, The activity coefficient of benzene in aqueous salt solutions, J. Am. Chem. Soc. 74 (7) (1952) 1773–1777.

[37] F. Hofmeister, About the science of the effects of salts: about the water withdrawing effect of the salts, Arch. Exp. Pathol. Pharmacol. 24 (1888) 247–260.
[38] B. Hribar, N.T. Southall, V. Vlachy, K.A. Dill, How ions affect the structure of water, J. Am. Chem. Soc. 124 (41) (2002) 12302–12311.
[39] D. Cheng, Y. Wen, L. Wang, X. An, X. Zhu, Y. Ni, Adsorption of polyethylene glycol (PEG) onto cellulose nano-crystals to improve its dispersity, Carbohydr. Polym. 123 (2015) 157–163.
[40] J.M. Passantino, A.D. Haywood, J. Goswami, V.A. Davis, Effects of polymer additives and dispersion state on the mechanical properties of cellulose nanocrystal films, Macromol. Mater. Eng. 302 (4) (2017) 1600351.
[41] Q. Beuguel, J.R. Tavares, P.J. Carreau, M.-C. Heuzey, Rheological behavior of cellulose nanocrystal suspensions in polyethylene glycol, J. Rheol. 62 (2) (2018) 607–618.
[42] M. Lin, V.S. Raghuwanshi, C. Browne, G.P. Simon, G. Garnier, Modulating transparency and colour of cellulose nanocrystal composite films by varying polymer molecular weight, J. Colloid Interface Sci. 584 (2021) 216–224.
[43] Y. Xu, A. Atrens, J.R. Stokes, Structure and rheology of liquid crystal hydroglass formed in aqueous nanocrystalline cellulose suspensions, J. Colloid Interface Sci. 555 (2019) 702–713.
[44] F. Pignon, M. Challamel, A. De Geyer, M. Elchamaa, E.F. Semeraro, N. Hengl, B. Jean, J.-L. Putaux, E. Gicquel, J. Bras, S. Prevost, M. Sztucki, T. Narayanan, H. Djeridi, Breakdown and buildup mechanisms of cellulose nanocrystal suspensions under shear and upon relaxation probed by SAXS and SALS, Carbohydr. Polym. 260 (2021) 117751.
[45] T. Cao, M. Elimelech, Colloidal stability of cellulose nanocrystals in aqueous solutions containing monovalent, divalent, and trivalent inorganic salts, J. Colloid Interface Sci. 584 (2021) 456–463.
[46] C. Metzger, D. Auber, S. Dähnhardt-Pfeiffer, H. Briesen, Agglomeration of cellulose nanocrystals: the effect of secondary sulfates and their use in product separation, Cellulose 27 (17) (2020) 9839–9851.
[47] R.M. Barajas-Ledesma, L. Hossain, V.N.L. Wong, A.F. Patti, G. Garnier, Effect of the counter-ion on nanocellulose hydrogels and their superabsorbent structure and properties, J. Colloid Interface Sci. 599 (2021) 140–148.
[48] M. Boström, D.F. Parsons, A. Salis, B.W. Ninham, M. Monduzzi, Possible origin of the inverse and direct Hofmeister series for lysozyme at low and high salt concentrations, Langmuir 27 (15) (2011) 9504–9511.
[49] A. Salis, F. Cugia, D.F. Parsons, B.W. Ninham, M. Monduzzi, Hofmeister series reversal for lysozyme by change in pH and salt concentration: insights from electrophoretic mobility measurements, PCCP 14 (13) (2012) 4343–4346.
[50] F.M. Menger, M.E. Chlebowski, Is the ether group hydrophilic or hydrophobic?, Langmuir 21 (7) (2005) 2689–2695